Density of superfluid helium droplets

Jan Harms and J. Peter Toennies
Max-Planck-Institut für Strömungsforschung, D-37073 Göttingen, Germany

Franco Dalfovo
Dipartimento di Fisica, Università di Trento, 38050 Povo, Italy
(Received 19 December 1997)

The classical integral cross sections of large superfluid ^4He_N droplets and the number of atoms in the droplets ($N=10^3-10^4$) have been measured in molecular beam scattering experiments. These measurements are in good agreement with the cross sections predicted from density functional calculations of the radial density distributions. By using a simple model for the density profile a 10–90 % surface thickness of about 6–8 Å is extracted directly from the data. [S0163-1829(98)02530-2]

I. INTRODUCTION

The study of the properties of ^{4}He clusters is currently an active area of theoretical and experimental research.[1,2] The interest is based on the fact that ^{4}He clusters provide an easily accessible example of a finite size quantum system of strongly correlated particles. One of the primary aims of He cluster research is to search for manifestations of superfluidity in mesoscopic systems. Recent spectroscopic studies of glyoxal molecules embedded in ^{4}He droplets with about 5000 atoms produced in free jet expansions give the first evidence that these droplets are indeed superfluid.[3] The internal temperature of these droplets has also been measured spectroscopically to be about 0.4 K (Ref. 4) in agreement with theory.[5]

Even though there has been notable progress in theoretical work on He clusters during the last few years the agreement between theory and experiments is not yet entirely satisfactory.[1] The implementation of *ab initio* calculations still remains difficult for inhomogeneous systems with more than a few hundred atoms, while phenomenological theories, which work well for describing macroscopic properties, are often not adequate for systems of finite size. In order to fill this gap density functional (DF) theories have been recently developed.[6]

The understanding of the density profiles in the surface region of a quantum fluid has long been considered a very important basic problem.[7] For this reason significant effort has gone into the experimental determination of the thickness of the bulk liquid-vapor ^{4}He interface.[7] At least three different experimental methods have been used to measure the surface thickness of bulk liquid He. The first involved atomic scattering experiments[8] yielding an interfacial width (10–90 %) of about 4 Å. A surface thickness of about 9 Å was measured with an ellipsometric method.[9] Finally, x-ray measurements give a surface thickness of the order of 8 Å, providing also information on the shape of the interface.[10] In droplets the surface atoms represent a significant fraction of the total number of atoms. For example, in a droplet with 5000 atoms about one half of the atoms are located in the surface region. Thus the physical properties of ^{4}He droplets are strongly influenced by the surface. Moreover, the surface region is particularly interesting because recent calculations predict that the Bose-condensed fraction, which in bulk ^{4}He is about 10%, approaches 100% in regions where the density is still within 10% of the bulk density.[11]

In this paper the liquid-vapor interface of large ^{4}He droplets ($N=10^3-10^4$) is investigated. The experiment consists in measuring both the integral cross section of the droplets and also their number size distributions. From the integral cross section and the average number of atoms an effective droplet volume as well as an average density is determined. The results are compared with theoretical predictions. Although a large number of calculations have been performed for the density profiles of small ^{4}He clusters ($N<10^3$)[1,12–18] no calculations for the large droplets investigated here have been reported so far. In the present work DF theory is used to calculate the density profiles of large ^{4}He droplets. The density functional used was recently introduced by the Orsay-Trento Collaboration.[6] This functional provides density profiles and energies[12] very close to the results of *ab initio* Monte Carlo calculations[13–15] in the case of small clusters and has the advantage that it can easily be applied to droplets with several thousands of atoms. These density profiles can be compared directly with the experimental data and good agreement is found within the experimental errors.

The droplet beam scattering apparatus is described in the following section. The procedure used to measure the number of atoms in the droplets and their classical integral cross sections are described in Secs. II A and II B. In Sec. II C the experimental results are presented and in Sec. III they are compared with the DF predictions. A final discussion is given in Sec. IV.

II. EXPERIMENT

Since the experimental methods and the apparatus used in this work have already been described in some detail in previous publications[19,20] the experimental procedure will be only briefly described here. The ^{4}He droplet beam is produced by a free jet expansion of ^{4}He from a stagnation source chamber at a high pressure and at low temperature (typically $P_0=5-100$ bar, $T_0=4-30$ K) through a thin walled (20 μm) nozzle with 5 ± 1 μm diameter. After the

droplets have passed the skimmer and several differential pumping stages they are scattered by a secondary beam produced in another free jet expansion beam source which crosses the droplet beam at an angle of 40°. The scattered droplets are detected with a home-made electron impact ionizer optimized for a high ionization efficiency followed by a magnetic mass spectrometer. The detector can be rotated around the scattering region in the plane of the two beams. To avoid capture collisions with the residual gas the background nonhelium pressures in the differential pumping stages between source and scattering chamber were kept below 10^{-7} mbar.

A. The number of atoms in the droplets

The atom number distribution $P(N)$ of the helium droplets is determined from the angular distribution resulting from scattering by the secondary beam. A small portion (5–10 %) of the droplets is deflected by the momentum transfer imparted by single collisions of the secondary beam gas atoms, most of which are captured by the droplets.[20]

The measurements described in the present study have been carried out at source pressures of $P_0=40$ bar and $P_0=80$ bar and nozzle temperatures between $T_0=13$ K and $T_0=26$ K. For these conditions the droplet velocity distributions are very narrow ($\Delta v/v\approx 2\%$) with well known mean speeds.[21] The secondary beam gases Ar and Kr were expanded from stagnation temperatures of about 300 K and several hundred millibar of stagnation pressure from a 40 μm diameter nozzle. The secondary beam contains no appreciable amount of dimers or larger clusters, and has a narrow velocity distribution ($\Delta v/v\approx 20\%$).

The angular distribution of the deflected droplet beam is measured by rotating the detector in small angular increments (typically 300 μrad) around the scattering center. Due to the large mass of the droplets the deflection angles are very small and a high angular resolution is necessary. This is achieved by collimating the incident beam with a 50 μm slit in front of the scattering center and a 25 μm slit in front of the detector. The width of the expansion zone and the broadening due to collisions with the residual background gas (mostly helium) leads to a full width at half maximum (FWHM) of the beam profile of about 1.5 mrad which defines the effective angular resolution.

Figure 1 shows three typical measured angular distributions with and without a flag in front of the secondary beam.[19] The small difference between the two signals is attributed to droplets which were deflected after capturing a secondary beam atom. Assuming complete momentum transfer the angle of deflection is directly dependent on the number of atoms in droplet. As is discussed in more detail below, the present experiments give further justification for the hypothesis of complete momentum transfer. The measured droplet atom number distributions can be very well fitted with a log-normal distribution[19,20]

$$P(N)=\frac{1}{\sqrt{2\pi}N\delta}\exp\left[-\frac{(\ln N-\mu)^2}{2\delta^2}\right], \tag{1}$$

where the mean number of atoms $\overline{N}$ and the width (FWHM) are

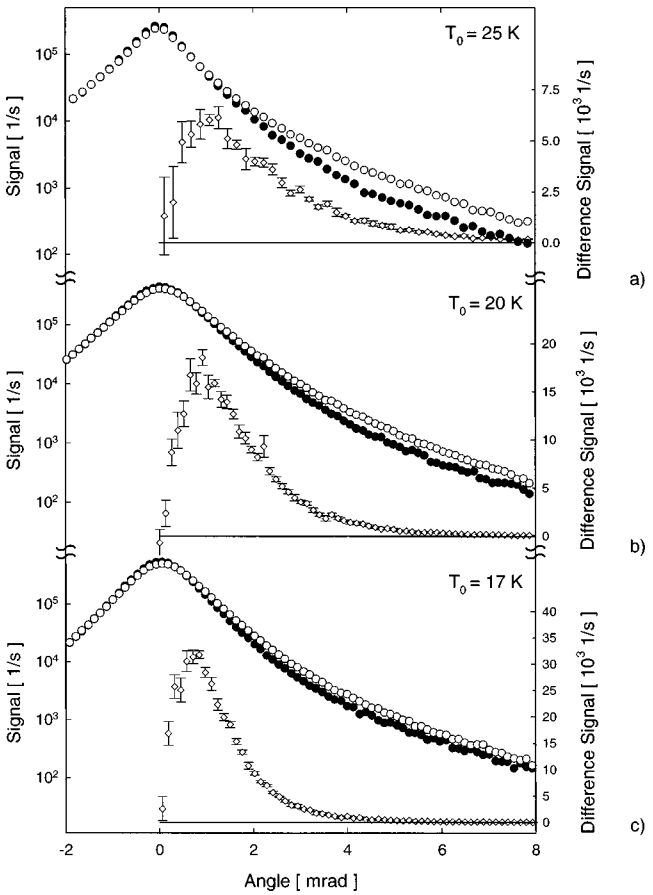

FIG. 1. Three typical measured angular distributions for a source pressure of $P_0=80$ bar and source temperatures of $T_0=25$ K (a), 20 K (b), and 17 K (c). Krypton was used as secondary beam gas. The signals with (filled circles) and without (open circles) a flag in front of the secondary beam are shown on a logarithmic scale. The weighted differences of the two signals (diamonds) with the standard deviations are shown on a linear scale. The mean number of atoms in the droplets are (a) $\overline{N}=2602$, (b) $\overline{N}=6174$, (c) $\overline{N}=9834$. The integral cross section is determined from the attenuation of the forward peak, i.e., 0 mrad.

$$\overline{N}=\exp\left(\mu+\frac{\delta^2}{2}\right) \tag{2}$$

and

$$\Delta N_{1/2}=\exp(\mu-\delta^2+\delta\sqrt{2\ln 2})-\exp(\mu-\delta^2-\delta\sqrt{2\ln 2}), \tag{3}$$

respectively. The FWHM is comparable with $\overline{N}$. Table I lists the results for $\overline{N}$, $\Delta N_{1/2}$, δ, and μ, measured using Ar and Kr as deflecting atoms for a wide range of different ^{4}He source pressures and temperatures. The values of $\overline{N}$ and $\Delta N_{1/2}$ obtained using Ar or Kr for identical ^{4}He source conditions do not always agree exactly, since they depend sensitively on the nozzle diameter and on the nozzle-skimmer distance which was optimized for each experiment and differed slightly. In particular the mean droplet sizes for $P_0=80$ bar with krypton as secondary gas are somewhat smaller by about 30% since the nozzle used in these experiments had a diameter of only about 4 μm as estimated from

TABLE I. Experimental results as function of source temperature (T_0), source pressure (P_0), and secondary gas. The mean number of atoms $\overline{N}$ and the half width $\Delta N_{1/2}$ are the results of fitting the measured mass distributions from the deflection experiment with a log-normal distribution [parameters δ and μ, see Eq. (1)]. The mean classical integral cross section $\overline{\sigma}$ is obtained by attenuation of the droplet beam with the secondary beam. From this data the mean density of the droplets $\overline{\rho}$ as a fraction of the known bulk density ($\rho_{\text{bulk}}=0.0218\ \text{Å}^{-3}$) is obtained directly.

T_0 [K]	P_0 [bar]	sec. gas	$\overline{N}$	$\Delta N_{1/2}$	δ	μ	$\overline{\sigma}$ [Å^2]	$\overline{\rho}/\rho_{\text{bulk}}$
24.0	40	Kr	703	667	0.426	6.46	2266	0.40
22.0	40	Kr	1700	1632	0.407	7.36	3138	0.59
20.0	40	Kr	2617	2373	0.528	7.73	4519	0.53
18.0	40	Kr	4700	4158	0.573	8.29	6259	0.58
17.0	40	Kr	6130	5331	0.603	8.54	7108	0.62
16.0	40	Kr	7741	6484	0.662	8.74	7661	0.70
15.0	40	Kr	8900	7719	0.607	8.91	8540	0.69
13.5	40	Kr	13 000	11 240	0.612	9.29	9538	0.85
26.0 [a]	80	Kr	1460	1298	0.565	7.13	3106	0.51
24.0 [a]	80	Kr	2700	2524	0.468	7.79	4111	0.62
18.0 [a]	80	Kr	5260	4374	0.673	8.34	6270	0.65
26.0	80	Ar	2114	1967	0.478	7.54	3431	0.64
24.0	80	Ar	3103	2835	0.514	7.91	4443	0.64
20.0	80	Ar	6458	5916	0.509	8.64	6615	0.70
18.0	80	Ar	9487	8530	0.544	9.01	9025	0.67

[a]The smaller cluster number sizes found with Kr instead of Ar as scattering gas at $P_0=80$ bar is a consequence of a smaller nozzle with an estimated diameter of about 4 μm.

the total gas flow into the nozzle chamber. These deviations however have no appreciable effect on the average densities. The latter depend on the number of atoms in the droplets and the integral cross sections, both of which are determined in the same experiment under identical source conditions (see below).

B. Integral cross sections

The integral cross sections of the droplets are determined by measuring the attenuation of the forward peak in the deflection pattern (see Fig. 1). The attenuation is related to the integral cross section $\overline{\sigma}$ of the droplets according to Beer's law[20]

$$\frac{I}{I_0}=\exp\left[-\frac{\overline{\sigma}n_{\text{sec}}L_{\text{eff}}v_{\text{rel}}F_{a0}}{v_{\text{drop}}}\right], \tag{4}$$

where I and I_0 are the intensities of the ^{4}He droplet beam with and without attenuation, n_{sec} is the number density of the secondary beam gas atoms in the scattering center, and L_{eff} is the effective length of the scattering volume. Moreover, v_{drop} is the speed of the droplets and v_{rel} the relative collision velocity. F_{a0} takes account of the smearing resulting from the velocity distributions of the two nozzle beams[22] and leads to a correction smaller than about 1%.

The product of the density in the scattering center and the effective length of the scattering volume ($n_{\text{sec}}L_{\text{eff}}$) was calibrated to within an error of approximately 5% by measuring the attenuation of a nearly monoenergetic helium atomic beam, for which the integral cross section can be accurately calculated quantum mechanically from the well-established interaction potential.[23] The density was calibrated three times with krypton and two times with argon at different collision energies and there was no evidence of systematic errors. The values of the absolute integral cross sections of the droplets are also listed in Table I.

The interpretation of the integral cross sections in Eq. (4) is straightforward only in the ideal case of an infinite angular resolution. In this case one gets the quantum-mechanical integral cross section, which includes the forward peaked diffraction part. In the present case of finite angular resolution the measured integral cross section is smaller since a fraction of the forward diffraction part of the differential cross section is not included. In order to estimate this correction, the quantum-mechanical differential cross section for elastic scattering was calculated using a partial wave expansion method.[24] The calculations, which are described in detail in Appendix A, indicate that the contribution of the diffraction part to the elastic cross section is negligible with the angular resolution of our apparatus. Thus the measured integral cross section $\sigma_{\text{app}}^{\text{int}}$ turns out to be very close to the classical cross section σ_{class}. The two cross sections agree to within 1% for droplets with 1000 atoms and for larger droplets the agreement is even better.

The finite width of the beam-profile also has the effect that the deflections of the largest droplets in the atom number distributions are too small to lead to a measurable attenuation of the beam. This error, however, can be estimated since the atom number distributions of the droplets and the beam profiles $S(\Theta)$ are both well known from the measurements. The calculation yields a correction of about 1% for mean atom numbers of 10^3 and of about 10% for droplets with 10^4 atoms.

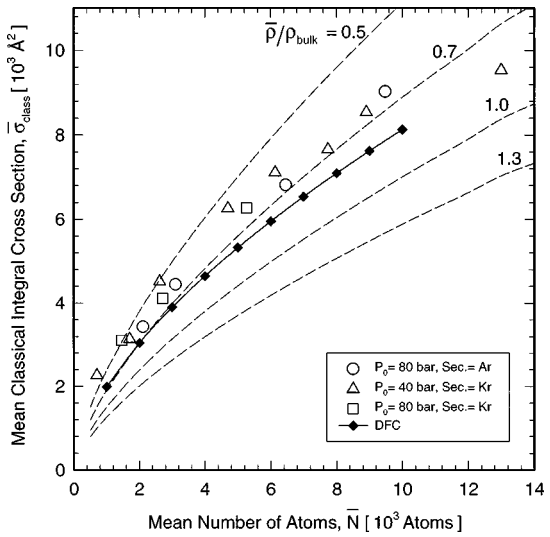

FIG. 2. The classical integral cross sections averaged over the measured number size distributions as functions of mean number of atoms $\bar{N}$. The empty symbols show the experimental results. The solid line with filled diamonds is the result of the DF calculations. For comparison, the mean classical cross sections of spherical droplets with constant density are indicated as dashed lines for different values of the density ($\rho_{\text{bulk}}=0.0218$ Å^{-3}). The different empty symbols indicate the different experimental parameters. Triangle: $P_0=40$ bar, secondary gas=Kr; square: $P_0=80$ bar, secondary gas=Kr; circle: $P_0=80$ bar, secondary gas=Ar.

C. Mean droplet densities

Measured values of the integral cross section $\bar{\sigma}$ as a function of the mean atom numbers $\bar{N}$ are reported in Fig. 2. The values obtained with argon and krypton as secondary gas fall on a common curve and so we can conclude that the integral cross section is independent of the nature of the secondary beam, within the estimated accuracy. The overall experimental errors are estimated to be about 5% and result mainly from the uncertainty in the determination of the density of the secondary beam atoms in the scattering volume.

From the measured cross section an effective mean density $\bar{\rho}$, defined as the density of a uniform sphere with a sharp step edge (liquid drop model) having the same classical integral cross section, is determined:

$$\bar{\rho}=\frac{3}{4}\sqrt{\frac{\pi}{\bar{\sigma}^3}}\bar{N}. \tag{5}$$

The values of $\bar{\rho}$, normalized to the bulk helium density $\rho_{\text{bulk}}=0.0218$ Å^{-3}, are given in the last column of Table I and the integral cross sections for spheres of different density are shown in Fig. 2 as dashed lines. Here the average integral cross section $\bar{\sigma}$ is calculated from the measured log-normal atom number distributions $P(N)$ by means of the following equation:

$$\overline{\sigma(\bar{N})}=\int_0^\infty P(N)\pi^{1/3}\left(\frac{3N}{4\bar{\rho}}\right)^{2/3}dN. \tag{6}$$

As can be seen, the experimental effective droplet density goes from about $0.5\rho_{\text{bulk}}$, for droplets with 10^3 atoms, to $0.7\rho_{\text{bulk}}$ for droplets with 10^4 atoms. This trend is consistent with the fact that a significant part of the atoms are in the outer surface region, where the density is less than the bulk density.

III. DENSITY PROFILES

The measured integral cross sections can be used to extract information about the density distribution $\rho(r)$. Since theoretical predictions of $\rho(r)$ were not available for such large droplets, density functional calculations using the improved functional recently developed in Ref. 6 are presented. In this approach, the energy of the system is assumed to be a functional of the particle density $E=\int d\mathbf{r}\mathcal{H}[\rho]$ and the equilibrium configuration is obtained by minimizing the energy with respect to ρ. The functional is written in the form

$$E=E_c[\rho]+\int d\mathbf{r}\frac{\hbar^2}{2m}(\nabla\sqrt{\rho})^2, \tag{7}$$

where the second term on the right-hand side is a quantum pressure, corresponding to the kinetic energy of a Bose gas of nonuniform density. The quantity $E_c[\rho]$ is a *correlation energy*, which incorporates the effects of dynamic correlations resulting from the interactions between the individual He atoms. The energy minimization then gives the nonlinear Schrödinger equation

$$\left\{-\frac{\hbar^2}{2m}\nabla^2+U[\rho,\mathbf{r}]\right\}\sqrt{\rho(\mathbf{r})}=\mu_4\sqrt{\rho(\mathbf{r})}, \tag{8}$$

where $U[\rho,\mathbf{r}]\equiv\delta E_c/\delta\rho(\mathbf{r})$ acts as a mean field, while the chemical potential μ_4 is introduced in order to ensure the proper normalization of the density to a fixed number of particles N. The density dependence of the correlation energy is parametrized in a phenomenological way, by choosing a functional form compatible with basic physical requirements and fixing a few parameters in accordance with the known properties of the bulk liquid. The detailed form of E_c is given in Appendix B. The DF theory is particularly suitable for the calculation of the density profiles of relatively large droplets. In fact, the density functional of Ref. 6 is accurate, by construction, in the limit of the uniform liquid. It also has been tested in the opposite limit of small clusters with 20–70 atoms[12] for which it provides density profiles in close agreement with *ab initio* Monte Carlo calculations.

The density profiles shown in the upper part of Fig. 3 are obtained by solving Eq. (8) for $N=10^3$–10^4. In order to estimate the contribution to the effective integral cross section σ_{eff} from the outer region of the theoretical profiles, the transmission coefficient $T(b)$ of the droplets is calculated as a function of the impact parameter b for argon and krypton using Beer's law [see the inset in Fig. 3(b)]. For this the trajectory of relative motion is integrated along a straight path $\mathbf{z}$, which is a good approximation in the outer region where the density is about 1% of the core density (see below):

$$T(b)=\exp\left(-\int_{\mathbf{z}(b)}\sigma(E_{\text{rel}})\rho(\mathbf{z})d\mathbf{z}\right). \tag{9}$$

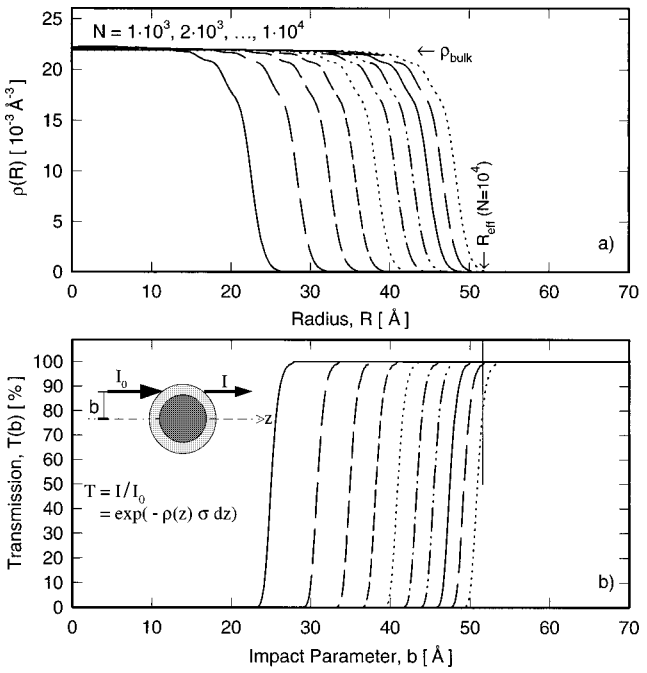

FIG. 3. The density distributions (a) calculated with a density functional method for droplets with between $N=10^3$ and $N=10^4$ atoms with steps of 10^3. The corresponding transmission for a beam of krypton or argon atoms is shown in (b). The effective radius $R_{\rm eff}$ for a droplet with 10^4 atoms is also indicated.

The atom-atom integral cross sections $\sigma(E_{\rm rel})$ were again calculated using the method given in Appendix A, with the relative velocities of the experiment. Here, the more realistic Tang-Toennies potentials[23] are used in place of the Lennard-Jones (12,6) potentials. The calculated transmission $T(b)$ of the droplets is illustrated in Fig. 3(b). The differences between argon and krypton are less than 1% and can therefore be neglected. The transmission for densities larger than about 10% of the central density is almost zero, so that the cross section is largely determined by the outer region of the droplet. Since the transmission rises very steeply the effective droplet-border is rather sharp and corresponds to a radius ($R_{\rm eff}$) where the density has fallen to approximately 1%. The integral cross section of the droplets is then calculated with the following equation:

$$\sigma_{\rm eff}=2\pi\int_0^\infty [1-T(b)]b\,db. \tag{10}$$

In a subsequent step the cross sections are averaged over the distribution in the number of atoms $P(N)$. The calculated results for the effective radii $R_{\rm eff}=\sqrt{\sigma_{\rm eff}/\pi}$, $\sigma_{\rm eff}$, the average relative densities $\overline{\rho}/\rho_{\rm bulk}$, and the 10–90 % thickness t are reported in Table II. The average relative densities $\overline{\rho}/\rho_{\rm bulk}$ in Fig. 2 (filled diamonds) lie between 0.64 and 0.8 and are somewhat larger than the experimental values by about 10–25 %. This discrepancy suggests that the theoretical surface thicknesses are somewhat smaller than the experimental values.

A simple model calculation can be used to check the effect of the surface thickness on the integral cross section. Since all theoretical calculations predict the core density of these large droplets to be equal to the bulk density, the density profile can be rather realistically described by a simple analytic function[25,26]

$$\rho(r)=\frac{\rho_{\rm bulk}}{2}\left[1-\tanh\left(2\frac{r-R}{g}\right)\right], \tag{11}$$

where R indicates the point where the density is reduced to 50% of the central density and g is a parameter controlling the surface thickness. By relating the density profile to the integral cross section using the same procedure described above, an experimental surface thickness is estimated by fitting the experimental cross section for the different droplets. The resulting values of t are shown in Fig. 4. We obtain a mean 10–90 % thickness of 6.4 ± 1.3 Å, which is somewhat larger than the results of the DF calculation (Table II) but

TABLE II. The effective radii $R_{\rm eff}=\sqrt{\sigma_{\rm eff}/\pi}$ and cross sections $\sigma_{\rm eff}$ obtained using Eq. (10) and DF calculations of density profiles. The effective density $\overline{\rho}$ as a fraction of the known bulk density ($\rho_{\rm bulk}=0.0218$ Å^{-3}) and the 10–90 % surface thickness t are listed.

N	$R_{\rm eff}$ [Å]	$\sigma_{\rm eff}$ [Å^2]	$\overline{\rho}/\rho_{\rm bulk}$	t [Å]
1000	25.75	2083	0.64	5.6
2000	31.59	3135	0.69	5.6
3000	35.69	4000	0.72	5.7
4000	38.94	4763	0.74	5.7
5000	41.69	5459	0.76	5.7
6000	44.09	6106	0.77	5.7
7000	46.22	6713	0.78	5.7
8000	48.18	7292	0.78	5.7
9000	49.97	7843	0.79	5.7
10 000	51.63	8373	0.80	5.7

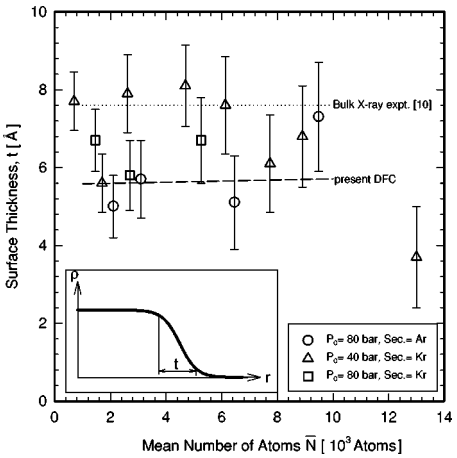

FIG. 4. The experimental 10–90 % surface thickness of He droplets as function of the mean number of atoms $\overline{N}$ assuming the symmetric density profile [Eq. (11)] shown in the inset. The mean value of t is 6.4 ± 1.3 Å. The DF values are shown as a dashed line and the value from the bulk x-ray experiment (Ref. 10) extrapolated to 0 K is shown as a dotted line. The different empty symbols indicate the different experimental parameters. Triangle: $P_0=40$ bar, secondary gas=Kr; square: $P_0=80$ bar, secondary gas=Kr; circle: $P_0=80$ bar, secondary gas=Ar.

TABLE III. The 10–90 % surface thickness of ^4He_N droplets and bulk liquid helium from different published experimental and theoretical works, where N is the number of atoms in the droplets and T the temperature (the values for $N=\infty$ refer to the planar free surface).

	N	method	T[K]	t[Å]
Osborne (Ref. 9)	∞	ellipsometry	1.8	9.4
Lurio *et al.* (Ref. 10)	∞	X-Ray	1.13	9.2
		extrapol.	0	7.6
Pandharipande *et al.* (Ref. 16)	<728	GFMC,VMC	0	5.5–7.2
Stringari, Treiner (Ref. 18)	<728	DF	0	8.8–9.2
	∞	DF	0	7
Sindzingre, Klein, Ceperley (Ref. 13)	64–128	PIMC	0.5–2	$\simeq 6$
Guirao, Centelles, Barranco *et al.* (Ref. 27)	∞	DF	0–4	6.5 (at 0.4 K)
Chin, Krotscheck (Ref. 14)	20–112	DMC	0	$\simeq 6$
	20–1000	HNC	0	$\simeq 6$
Barnett, Whaley (Ref. 15)	<112	DMC	0	$\simeq 6$

still within the error limits. One has to stress here that the results are dependent on the model used for $\rho(r)$; in particular, it assumes a symmetric density profile. Most of the predicted density profiles are, however, slightly asymmetric, with a steeper slope in the outer part of the surface. By using an asymmetric profile, with an asymmetry similar to the one of the DF profiles in Fig. 3, the estimated surface thickness is about 1–2 Å larger than the values shown in Fig. 4.

IV. DISCUSSION

The experimental and theoretical results for the surface thickness of the bulk and droplets are compared in Table III with several other calculations for smaller droplets and the bulk liquid surface. The present DF calculations for large droplets predict a surface thickness $t \cong 5.7$ Å (see also Table II) which is slightly less than other calculations. For example, previous DF calculations for a planar free surface[27] gave $t \cong 7$ Å, while from *ab initio* calculations on small clusters[13–18] values between 6 and 7 Å are predicted. It is also worth mentioning that the recent measurements of Ref. 10 suggest an even larger thickness, but the value extrapolated to $T=0$ is still compatible with the present results within the accuracy (see Fig. 4).

Since the differences between the experiment and theory in the average densities shown in Fig. 2 are greater than the experimental statistical uncertainties, which are expected to be less than $\pm 5\%$, the possible sources of systematic errors have to be considered. The possibility that the measured droplet atom numbers $\overline{N}$ are too small, which would shift the mean effective density to smaller values, seems unlikely. This would require a momentum transfer in the deflection experiment even larger than the momentum $\mathbf{p}_{\rm sec}$ of the impinging secondary atom. For elastic backscattering of the atoms in central collisions from a hard sphere the momentum transfer would indeed be $2\mathbf{p}_{\rm sec}$. The momentum transfer averaged overall impact parameters for elastic scattering from a hard sphere is, however, equal to the momentum of the incoming particle $\mathbf{p}_{\rm sec}$. Thus even in the unlikely case of elastic recoil scattering, which in view of the large mass of the argon and krypton atom compared to that of the He atom seems very unlikely and is not even expected for the scattering from a liquid helium surface,[8] the same results would still hold. Recoil scattering would also be in contradiction to the observation that the secondary gas is captured by the He droplets and that the measured angular distributions of the deflected droplets are the same, independent of whether they are detected on the mass of the He_2^+ ion fragments or on the mass of the particles picked up from the secondary beam.[19,20] Another possibility is a backward directed vaporization of helium induced by the impinging secondary gas atom, as proposed by Gspann.[28] According to ordinary fluid dynamics this would also seem implausibly, since the impact speeds are greater than the velocity of first sound of about 240 m/s (Ref. 28) and therefore a conical Mach shock should be created which degenerates into a spherical sound wave. This sound wave would more probably induce vaporization in the forward direction which would tend to shift our results to greater droplet atom numbers $\overline{N}$ and would increase the discrepancy with the theoretical results.

Another possibility is that the measured cross sections are affected by elastic processes. As discussed in Appendix A the scattering from the effective long range potential leads only to a small increase ($<1\%$) of the measured integral cross sections compared with the classical cross sections. On the other hand, glancing collisions in which the atoms approach the droplet surface at small angles of incidence could conceivably also undergo an elastic collision and not contribute to the measured integral cross section. An upper limit on this effect can be estimated by assuming that the reflectivity of Ar and Kr from liquid He surfaces is equal to the reflectivity of ^{4}He, which can be estimated from experiments.[8] The reflectivity of ^{4}He at the relative speeds of $v_{\rm rel} \approx 400$ m/s used here is small and is expected to be larger than 10^{-2} only for angles of incidence smaller than about 5°. Even if the reflectivity were unity the overall effect would be less than about 1%.

At finite temperatures the surface will be additionally broadened (finite-T broadening) by the excitations of the surface vibrational modes which have frequencies of the order of 0.1 K (Ref. 14) well below the temperature of the droplets. These vibrations could increase the cross section with respect to the one of spherical droplets at $T=0$. This effect also seems to be small since, for example, the path-integral

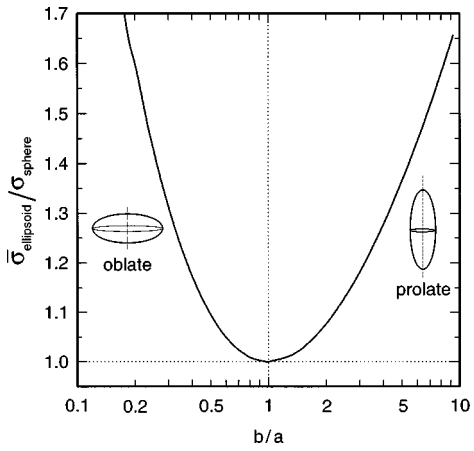

FIG. 5. The effective integral cross section of an ellipsoid averaged over all possible orientations in units of the cross section of a sphere with the same volume. The radius b is the axis of symmetry and a indicates the other radius.

Monte Carlo calculations of Ref. 13 for small droplets at $T=0.5$ K, which include the finite-T broadening, show a density profile very similar to the other Monte Carlo calculations at zero temperature. At the other extreme of a planar free surface (see Table III), the calculations of Ref. 27 give again an almost temperature-independent profile up to 1 K. Thus, even though direct theoretical estimates of the finite-T broadening for large clusters are not yet available, this effect is expected to be negligible at the low temperature of the droplets, 0.4 K.

A final source of experimental error could arise from a nonspherical shape of the droplet. Such a distortion might result from the large angular momentum (several 1000 $\hbar$) which some of the droplets may have as a result of collisions with the residual gas before arriving in the scattering region. A simple estimate indicates that in view of the large mass of the droplet, the resulting rotation speed is slow compared with the colliding secondary beam atoms and thus the droplets can be considered as being stationary during the collision. Thus the effect of a possible deformation on the experimental results can be estimated from the calculated geometrical cross section of a rotational ellipsoid averaged over all orientations.

The radius of the ellipsoid is assumed to have the length a and the radius of the axis of rotational symmetry is given by b. For $a>b$ one gets an oblate and for $a<b$ a prolate ellipsoid. The geometrical cross section σ_{ell} under an angle of view ω can be written as (see Appendix C)

$$\sigma_{ell}=\frac{4}{3}\pi a\sqrt{\frac{b^4+a^4\tan^2\omega}{b^2+a^2\tan^2\omega}}\sin\left[\omega+\arctan\left(\frac{b^2}{a^2\tan\omega}\right)\right]. \tag{12}$$

The effective cross section is obtained by averaging numerically over all orientations,

$$\overline{\sigma_{ell}}=\frac{1}{2}\int_0^{\pi}d\omega\,\sin(\omega)\sigma_{ell}(\omega). \tag{13}$$

The resulting mean cross section is shown as a function of the ratio of the radii b/a in Fig. 5, scaled to the cross section of a sphere with the same volume. For a real droplet with lower density at the surface the effect will be even greater, since the surface area of the ellipsoid is larger. To explain the difference of 5–10 % between the DF results and the experiments, oblate shaped droplets with a value of $b/a\approx 0.6$ or prolate droplets with $b/a\approx 2.5$ would be required. Oblate shapes with such small average b/a ratios seem unlikely in view of the relatively small fraction ($\approx 15\%$) of the incident beam droplets which undergo collisions with the residual gas. Thus we conclude that even in the very unlikely case that the droplets are somewhat distorted this has little effect on the measured surface thickness.

In summarizing these considerations of experimental shortcomings it appears that the systematic errors in our experimental results are quite small and comparable to the statistical errors of $\pm 5\%$. The discrepancy of the order of 10–20 % indicated by the comparison with the theoretical values probably originates from some more fundamental shortcomings in the DF method. This conclusion is supported by the comparisons between DF calculations for the bulk liquid surface and experiments listed in Table III for which a similar discrepancy is found.

Finally it is interesting to note that the same qualitative agreement between the measured cross sections and those obtained from the DF calculations over the entire range of number sizes provides evidence in support of the trend seen in the calculations that the width of the surface profile does not change with droplet size. This observation and the comparisons in Table III all suggest that the true surface thickness of these large droplets could also be estimated from calculations of much smaller clusters with at least 100 atoms for which the central density is invariably predicted to be equal to the bulk density.

V. CONCLUSIONS

By using a combination of scattering techniques (deflection and attenuation), it has been possible to measure the average densities of large helium droplets with $N=10^3$ to 10^4 atoms. These results have been compared with density functional calculations. Overall agreement can be considered to be satisfactory but on closer examination the predicted effective integral cross sections are too small by about 10–20 % and the mean densities too large by about 10–25 %, which is larger than the errors which are estimated to be about $\pm 5\%$. An attempt to fit the experimental data using a symmetric model density profile yields a value for the 10–90 % thickness of $t=6.4\pm 1.3$ Å which is larger than the density functional value of 5.7 Å and is consistent with the differences in the average densities. The assumptions made in the analysis were critically examined and an explanation for the small discrepancy cannot be at present provided. As discussed in connection with Table III the situation is similar to the surface of the bulk where experiments also yield thicknesses which are larger than predicted by most theories. The experimental method has also been recently applied to ^{3}He droplets[29] and there the average densities relative to the bulk are even smaller than found here for ^{4}He, a trend which is consistent with recent Thomas-Fermi theoretical calculations.[30]

In the future it is conceivable that the present experimen-

tal method can be further improved to provide a sensitive quantitative probe of the outer surface region of large droplets. Here it is interesting to speculate what effect the large condensate fraction in this outer region[11] would have on the cross section. One can also explore the existence of a Landau velocity below which the interaction should disappear, as it happens in the bulk liquid at 57 m/s. Experiments under such conditions are now possible[31] and are envisaged in the future.

ACKNOWLEDGMENTS

The authors are grateful to B. Schilling for his contribution to the early phases of this work. They thank U. Henne and M. Lewerenz for many valuable discussions and M. Faubel and B. Whaley for their critical reading of the manuscript.

APPENDIX A: INTEGRAL CROSS SECTION

The quantum-mechanical differential cross section for elastic scattering from the secondary beam gas atoms was calculated using a partial wave expansion method[24] in order to estimate the effect of the forward diffraction contribution on our results. The following spherical model potential obtained by integrating the Lennard-Jones 12-6 potential between the scattering atom and the He atoms of the droplet was assumed:[32]

$$V_N(r)=\frac{4N\varepsilon\kappa^6}{(r^2-R^2)^3}\left[\frac{\kappa^6\left(r^6+\frac{21}{5}r^4R^2+3r^2R^4+\frac{1}{3}R^6\right)}{(r^2-R^2)^6}-1\right];\quad r>R. \tag{A1}$$

The integration is simplified by assuming the He atoms to be homogeneously distributed within a sphere of radius R. Here the effective radius R corresponds to the radius $R_N=r_0N^{1/3}$ of a droplet with N atoms reduced by the effective radius r_0 of one atom in the same droplet, i.e., $R=R_N-r_0=(N^{1/3}-1)r_0$. Estimates of the effective radius r_0 of one helium atom in a droplet can be extracted from quantum many-body calculations. For instance, Pandharipande *et al.*[16] reported the value $r_0(N)=2.24+0.38N^{-1/3}+2.59N^{-2/3}$. The parameters ε and κ are such that, in the limiting case $N=1$, the potential V_N reduces to the two-body Lennard-Jones He-Kr or He-Ar potential

$$V_1(r)=4\varepsilon[(\kappa/r)^{12}-(\kappa/r)^6]\equiv\varepsilon\left[\left(\frac{R_m}{r}\right)^{12}-2\left(\frac{R_m}{r}\right)^6\right], \tag{A2}$$

where $R_m=2^{1/6}\kappa$. We use $\varepsilon=2.67$ meV and $R_m=3.70$ Å for He-Kr, and $\varepsilon=2.59$ meV and $R_m=3.40$ Å for He-Ar.[33] Although the inner repulsive potential is not realistic for central collisions with the strongly absorbing liquid core of the He droplet, the potential Eq. (A1) should be a good approximation for describing the glancing collisions, which are the relevant ones in determining the elastic contribution to the integral cross section.

The integral cross section of real He droplets consists of the elastic cross section σ_e resulting from diffraction in large impact collisions and the absorption cross section σ_a in more central collisions. In the calculations with the hard core potential Eq. (A1) the angularly distributed isotropic part of the differential cross section takes account of the effect of the absorption cross section σ_a. In our case, where the de Broglie wavelength of relative motion λ is much smaller than the droplet radius, all particles with impact parameter smaller than approximately R_N are expected to be absorbed. The contribution of particles with angular momentum l to the cross section is given by $\sigma_l=(2l+1)\pi\lambda^2$.[34] Then the integral cross section is given approximately by

$$\sigma\simeq\sum_{l=0}^{R_N/\lambda}(2l+1)\pi\lambda^2+\sum_{l=R_N/\lambda}^{\infty}\sigma_{el,l}\simeq\pi R_N^2+\sigma_e. \tag{A3}$$

The part σ_e was calculated quantum mechanically exactly for the potential Eq. (A1). Since the calculated elastic scattering is found to be sharply peaked in the forward direction its contribution to the integral cross section can be neglected for center of mass angles ϑ larger than about 5°. The laboratory scattering angle Θ is in the case of $m_{\rm drop}\gg m_{\rm sec}$ related to ϑ by

$$\Theta(\vartheta)=\frac{m_{\rm sec}}{v_{\rm drop}(m_{\rm sec}+m_{\rm drop})}\left\{v_{\rm rel}\sin\left[\arcsin\left(\frac{v_{\rm sec}\sin\beta}{v_{\rm rel}}\right)+\vartheta\right]-v_{\rm sec}\sin\beta\right\}, \tag{A4}$$

where $v_{\rm rel}$ is the relative speed of the two beams and β is the angle between them. Since the mass $m_{\rm drop}$ of the primary beam droplets is much larger than the mass $m_{\rm sec}$ of the secondary gas atoms the angle Θ turns out to be very small. For example, a center of mass angle $\vartheta=5°$ corresponds to laboratory angles Θ of about 1 mrad for droplets with 1000 atoms, which is comparable with the angular resolution of our apparatus.

The theoretical differential cross sections were convoluted with the angular distributions $S(\Theta)$ of the incident beam (beam profiles). These latter angular distributions were measured with the same method as described in Sec. II A with the secondary beam blocked with a beam flag located in the scattering chamber. In this arrangement the residual gas pressure and its effect on the beam profile is the same as in the scattering experiment. The predicted effective integral cross section is then given by

$$\sigma_{\rm app}^{\rm int}=2\pi\int_{\vartheta_{\rm app}}^{\pi}d\vartheta\,\sin(\vartheta)\left\{\int_{-\pi}^{\pi}d\zeta\left(\frac{d\sigma(\vartheta-\zeta)}{d\omega}\right)_{\rm th}s(\zeta)\right\}, \tag{A5}$$

where the $\vartheta_{\rm app}$ represents the effective geometrical center of mass resolution given by the slit in front of the scattering center and in front of the detector and $s(\vartheta)$ is the measured angular profile of the unscattered beam transformed into the center of mass system. The quantity $(d\sigma/d\omega)_{\rm th}$ is the calculated elastic differential cross section. Fortunately the resulting value of $\sigma_{\rm app}^{\rm int}$ turns out to be very close to the classical cross section $\sigma_{\rm class}=\pi R_N^2$; the two cross sections agree to within 1% for droplets with 1000 atoms and for larger drop-

lets the agreement is even better. Thus the corrections discussed above justify the assumption that the classical cross section is measured.

APPENDIX B: DENSITY FUNCTIONAL

The explicit expression of the correlation energy E_c, entering the density functional (7), is given by[6,12]

$$E_c[\rho]=\int d\mathbf{r}\left\{\frac{1}{2}\int d\mathbf{r}'\rho(\mathbf{r})V_l(|\mathbf{r}-\mathbf{r}'|)\rho(\mathbf{r}')+\frac{c_2}{2}\rho(\mathbf{r})\times[\overline{\rho_h(\mathbf{r})}]^2+\frac{c_3}{3}\rho(\mathbf{r})[\overline{\rho_h(\mathbf{r})}]^3-\frac{\hbar^2}{4m}\alpha_s\int d\mathbf{r}'\ F(|\mathbf{r}-\mathbf{r}'|)\left(1-\frac{\rho(\mathbf{r})}{\rho_{0s}}\right)\times\nabla\rho(\mathbf{r})\cdot\nabla\rho(\mathbf{r}')\left(1-\frac{\rho(\mathbf{r})}{\rho_{0s}}\right)\right\}. \tag{B1}$$

The two-body interaction V_l is the Lennard-Jones interatomic potential, with the standard parameters $\alpha=2.556$ Å and $\varepsilon=10.22$ K, screened at short distance ($V_l\equiv 0$ for $r<h$, with $h=2.1903$ Å). The two terms with the parameters $c_2=-2.411\,857\times10^4$ K Å^6 and $c_3=1.858\,496\times10^6$ K Å^9 account phenomenologically for short-range correlations between atoms. The weighted density $\overline{\rho_h(\mathbf{r})}$ is the average of ρ over a sphere of radius h centered in $\mathbf{r}$. The last term, depending on the gradient of the density in different points, is introduced to reproduce the static response function in the roton region. The function F is a simple Gaussian $F(r)=\pi^{-3/2}\ell^{-3}\exp(-r^2/\ell^2)$ with $\ell=1$ Å, while $\alpha_s=54.31$ Å^3 and $\rho_{0s}=0.04$ Å^{-3}.

APPENDIX C: MEAN GEOMETRICAL CROSS SECTION OF A ROTATIONAL ELLIPSOID

A rotational ellipsoid is assumed with the axis of rotational symmetry b parallel to the z axis and the other two radii a:

$$\frac{x^2+y^2}{a^2}+\frac{z^2}{b^2}=1. \tag{C1}$$

This can be written in spherical coordinates

$$r(\Theta,\Phi)=\frac{b}{1-\epsilon^2\sin^2(\Theta)},\quad \epsilon=\frac{\sqrt{a^2-b^2}}{a}<1. \tag{C2}$$

Since the visible cross section $\sigma_{\rm ell}$ of the ellipsoid from a viewing point with a polar angle ω does not depend on the azimuth angle Φ, the problem can be reduced to the x-z plane. The visible cross section $\sigma_{\rm ell}$ is given by the projection of the cutting plane through the ellipsoid which is defined by the tangents with angle ω. Since every cutting plane of an ellipsoid is an ellipse, the area of the cutting plane σ_s can be written as

$$\sigma_s(\omega)=\pi a r_s(\omega). \tag{C3}$$

The projection on a plane perpendicular to the viewing direction is given by

$$\sigma_{\rm ell}(\omega)=\sigma_s(\omega)\cos(\omega-\Theta_s). \tag{C4}$$

To find the vector $\mathbf{r}_s=\binom{r_s}{\pi-\Theta_s}=\binom{x_s}{z_s}$ lying in the cutting plane the equation of a tangent at the ellipse has to be calculated:

$$1=\frac{xx_s}{a^2}+\frac{zz_s}{b^2} \tag{C5}$$

which yields

$$z=\frac{b^2}{z_s}-\frac{b^2x_s}{a^2z_s}x. \tag{C6}$$

The tangent must be parallel to the viewing direction ω:

$$\cot(\omega)=\frac{dz}{dx}=-\frac{b^2x_s}{a^2z_s}. \tag{C7}$$

With Eq. (C1) follows

$$x_s^2=\frac{a^4\cot^2(\omega)}{b^2+a^2\cot^2(\omega)}, \tag{C8}$$

and for z_s and r_s

$$z_s^2=\frac{b^4}{b^2+a^2\cot^2(\omega)}, \tag{C9}$$

$$r_s^2=x_s^2+z_s^2=\frac{b^4+a^4\cot^2(\omega)}{b^2+a^2\cot^2(\omega)}. \tag{C10}$$

From Eqs. (C8) and (C9) Θ_s can be calculated:

$$\tan(\Theta_s)=\frac{z_s}{x_s}=\frac{b^2}{a^2\cot(\omega)}. \tag{C11}$$

The visible cross section of an ellipsoid follows from Eqs. (C3) and (C4):

$$\sigma_{\rm ell}(\omega)=\pi a\sqrt{\frac{b^4+a^4\cot^2(\omega)}{b^2+a^2\cot^2(\omega)}}\times\cos\left[\omega-\arctan\left(\frac{b^2}{a^2\cot(\omega)}\right)\right]. \tag{C12}$$

The mean cross section is derived by integration over ω:

$$\overline{\sigma_{\rm ell}(\omega)}=\frac{1}{2}\int_0^\pi d\omega\ \sin(\omega)\sigma_{\rm ell}(\omega). \tag{C13}$$

[1] K. B. Whaley, Int. Rev. Phys. Chem. **13**, 41 (1994).
[2] J. P. Toennies, in *Proceedings of the International School of Physics Enrico Fermi on ''Chemical Physics of Atomic and Molecular Clusters,'' Course CVII*, edited by G. Scoles (North Holland, Amsterdam, 1990), p. 597 f.
[3] M. Hartmann, F. Mielke, J. P. Toennies, A. Vilesov, and G. Benedek, Phys. Rev. Lett. **76**, 4560 (1996).
[4] M. Hartmann, R. E. Miller, J. P. Toennies, and A. Vilesov, Phys. Rev. Lett. **75**, 1566 (1995).
[5] D. M. Brink and S. Stringari, Z. Phys. D **15**, 257 (1990).
[6] F. Dalfovo, A. Lastri, L. Pricaupenko, S. Stringari, and J. Treiner, Phys. Rev. B **52**, 1193 (1995).
[7] D. O. Edwards and W. F. Saam, in *Progress in Low Temperature Physics*, edited by D. F. Brewer (North Holland, Amsterdam, 1978), Vol. 7A, Chap. 4.
[8] V. U. Nayak, D. O. Edwards, and N. Masuhara, Phys. Rev. Lett. **50**, 990 (1983).
[9] D. V. Osborne, J. Phys.: Condens. Matter **1**, 289 (1989).
[10] L. B. Lurio, T. A. Rabedeau, P. S. Pershan, I. F. Silvera, M. Deutsch, S. D. Kosowsky, and B. M. Ocko, Phys. Rev. Lett. **68**, 2628 (1992).
[11] A. Griffin and S. Stringari, Phys. Rev. Lett. **76**, 259 (1995).
[12] M. Casas, F. Dalfovo, A. Lastri, L. Serra, and S. Stringari, Z. Phys. D **35**, 67 (1995).
[13] P. Sindzingre, M. L. Klein, and D. M. Ceperley, Phys. Rev. Lett. **63**, 1601 (1989).
[14] S. A. Chin and E. Krotscheck, Phys. Rev. B **45**, 852 (1992); **52**, 10 405 (1995).
[15] R. N. Barnett and K. B. Whaley, Phys. Rev. A **47**, 4082 (1993); M. A. McMahon, R. N. Barnett, and K. B. Whaley, J. Chem. Phys. **104**, 5080 (1996).
[16] V. R. Pandharipande, J. G. Zabolitzky, S. C. Pieper, R. B. Wiringa, and U. Helmbrecht, Phys. Rev. Lett. **50**, 1676 (1983).
[17] V. R. Pandharipande, S. C. Pieper, and R. B. Wiringa, Phys. Rev. B **34**, 4571 (1986).
[18] S. Stringari and J. Treiner, J. Chem. Phys. **87**, 5021 (1987).
[19] M. Lewerenz, B. Schilling, and J. P. Toennies, Chem. Phys. Lett. **206**, 381 (1993).
[20] M. Lewerenz, B. Schilling, and J. P. Toennies, J. Chem. Phys. **102**, 8191 (1995).
[21] H. Buchenau, J. P. Toennies, and J. Northby, J. Chem. Phys. **95**, 8134 (1991).
[22] K. Berkling, R. Helbing, K. Kramer, H. Pauly, Ch. Schlier, and P. Toschek, Z. Phys. **166**, 406 (1962).
[23] K. T. Tang and J. P. Toennies, Z. Phys. D **1**, 91 (1986).
[24] D. Eichenauer, A. Scheidemann, and J. P. Toennies, Z. Phys. D **8**, 295 (1988).
[25] R. M. Townsend, J. Gryko, and J. Rice, J. Chem. Phys. **82**, 4391 (1985).
[26] J. Jortner, Z. Phys. D **24**, 247 (1992).
[27] A. Guirao, M. Centelles, M. Barranco, M. Pi, A. Polls, and X. Vinas, J. Phys.: Condens. Matter **4**, 667 (1992).
[28] J. Gspann, Physica B **108**, 1309 (1981).
[29] J. Harms and J.P. Toennies (unpublished).
[30] M. Barranco (private communication).
[31] J. Harms, E. L. Knuth, and J. P. Toennies, J. Chem. Phys. **106**, 3348 (1997).
[32] J. Gspann and H. Vollmar, *Rarefield Gas Dynamics* (Academic, New York, 1974), Vol. 93.
[33] L. J. Danielson and M. Keil, J. Chem. Phys. **88**, 851 (1988).
[34] J. M. Blatt and V. F. Weisskopf, *Theoretical Nuclear Physics* (Springer Verlag, New York, 1979), Sect. VIII, p. 317.